Rare Metal Materials and Engineering
Volume 52, Issue 1, January 2023
Available online at www.rmme.ac.cn

Science Press

Cite this article as: Yang Bowen, Ma Chuanchuan, Xue Chun, et al. Effect of Initial Texture on Twinning and Texture Evolution of AZ31 Magnesium Alloy[J]. Rare Metal Materials and Engineering, 2023, 52(01): 125-132.

ARTICLE

Effect of Initial Texture on Twinning and Texture Evolution of AZ31 Magnesium Alloy

Yang Bowen, Ma Chuanchuan, Xue Chun, Tuo Leifeng, Gui Hailian, Chu Zhibing

School of Materials Science and Engineering, Taiyuan University of Science and Technology, Taiyuan 030024, China

Abstract: To study the deformation twins and plastic anisotropy of AZ31 magnesium alloy, based on the plastic constitutive theory of rate-correlated crystals, a magnesium alloy model with different initial textures, including slip and twin deformation mechanisms, was established by the finite element method. Besides, the volume fraction of twin crystals was introduced into the model. The relationship among texture evolution, twins, and mechanical properties during compression was studied. Results show that the plastic behavior of crystal depends largely on the initial texture, and the difference in the initial texture leads to the obvious anisotropy of compression behavior: high axial yield and tensile strength and low radial yield and tensile strength. During the compressive plastic deformation process, with increasing the deformation, the volume fraction of activated twin crystal is increased. In addition, the higher the volume fraction of radial compressive activated twin crystal, the lower the volume fraction of axial compressive activated twin crystal. The points of obvious twin crystal appearance in the simulation coincide with those of stress mutation. When the volume fraction of twin crystal reaches a certain value, the stress suddenly changes, the crystal orientation changes significantly, and the new slip system is activated, reflecting the influence of the coupling of slip and twin crystal mechanisms on the mechanical properties of AZ31 magnesium alloy.

Key words: AZ31 magnesium alloy; crystal plasticity finite element; initial texture; twin crystal; mechanical property

Magnesium alloy is widely used as structural material in aerospace, communication electronics, automobile, and other fields due to its lightweight, high specific strength and stiffness, good cutting and casting performance, abundant sources, and easy recovery[1–3]. In the forming process of metal materials, different textures usually form, such as extruded bars. In the process of plastic deformation, the textures often slip along the crystal plane with the densest atoms, and the crystal and slip plane usually rotate, resulting in the partially ordered grains in polycrystals. The preferred orientation of directly generated grains is referred as deformation texture[4–6]. Texture can directly affect the physical and mechanical properties of materials. After texture forms in the magnesium alloy, the obvious anisotropy at room temperature can be observed. The texture strengthening of magnesium alloy is a common method to improve the mechanical properties and forming properties[7–10].

Taylor et al[11] developed the crystal plasticity theory based on the quantitative analysis and proposed the kinematic equation and constitutive model of single crystal plastic deformation. On this basis, Asaro[12–13], Peirce[14], and Hill[15] et al introduced the concepts of self-hardening and latent hardening to describe the interaction of dislocations in the same/different slip systems and established a complete crystal plasticity theory. Among them, the crystal hardening theory mainly includes the rate-independent and rate-correlated[16–18] crystals. The work hardening of common metal materials is related to the loading rate. The rate-correlated crystal material hardening theory was adopted in this research. Recently, the crystal plasticity theory has been widely researched. Li et al[19] studied the effects of anisotropy and tension-compression asymmetry on the formability of materials by establishing a constitutive model. Shi et al[20] used in-situ electron backscatter diffractometer (EBSD) and found that with

Received date: April 25, 2022
Foundation item: National Key Research and Development Project (2018YFB1307902); National Natural Science Foundation of China (52175353); Shanxi Young Top Talent Project, Shanxi Province Science Foundation for Youths (201901D211312); Excellent Young Academic Leaders in Shanxi Colleges and Universities (2019045); Excellent Achievements Cultivation Project of Shanxi Higher Education Institutions (2019KJ028); Shanxi Graduate Education Innovation Project (2019SY482); Key Research and Development Projects of Shanxi Province (201903D121043)
Corresponding author: Chu Zhibing, Ph. D., Professor, School of Materials Science and Engineering, Taiyuan University of Science and Technology, Taiyuan 030024, P. R. China, Tel: 0086-351-2776763, E-mail: chuzhibing@tyust.edu.cn

increasing the deformation, the twins of AZ31 magnesium alloy gradually expand to the equiaxed crystal boundary, therefore affecting the grain boundary and causing twin nucleation in adjacent grains to coordinate deformation. Wang et al[21] revealed the effects of different strain rates on twin density and dislocation density. Lan et al[22] revealed the effect of loading direction on plastic deformation behavior by applying loading of different directions onto single crystal AZ31 magnesium alloy. Su et al[23] investigated the mechanism of tensile asymmetry caused by different deformation mechanisms of the magnesium alloy with initial extruded silk texture through a modified viscoplastic self-consistent model. Based on the crystal plasticity theory, a single-crystal plastic constitutive model of AZ31 magnesium alloy with different initial textures was established, including the slip and twinning mechanisms. In addition, the volume fraction of twin crystal[24–25] was introduced into this model.

Thus, in order to study the effects of initial textures on the twins, texture evolution, and mechanical properties of AZ31 magnesium alloy during the compression process, the magnesium alloy models were established based on the crystal plasticity finite elements. The deformation textures of magnesium alloys during the compressive process could be achieved via the user-defined material interface (UMAT) in finite element software. In order to verify the crystal plasticity finite element model, cubic specimens along the axial and radial directions were cut from the extruded AZ31 magnesium alloy bar, and the uniaxial compression experiment was conducted. The microstructure and deformed texture were characterized by EBSD and then compared with the simulation results. This research provided a theoretical basis for processing and development of magnesium alloy.

1 Crystal Plastic Constitutive Model

1.1 Crystal plastic constitutive relation

Based on the crystal plasticity constitutive model, the corotational stress rate ($\bar{\sigma}$) of Cauchy stress with the material coordinate axis was established with the lattice elastic deformation rate tensor D^* [26], as follows:

$$\bar{\sigma} + (\Omega - \bar{\Omega})\sigma - \sigma(\Omega - \Omega^*) + \sigma(I{:}D^*) = L{:}D^* \tag{1}$$

where σ is the stress; I is the second-order unit tensor; L is the elastic tensor; Ω is the antisymmetric spin tensor; Ω^*means decomposable tensor into lattice parts.

The crystal slip obeys Schmidt criterion. Thus, the slip ratio of arbitrary slip system α ($\dot{\gamma}^{(\alpha)}$) depends on the Schmidt stress with current stress σ:

$$\tau^{(\alpha)} = m^{*(\alpha)}\frac{\rho_0}{\rho}\sigma s^{*(\alpha)} \tag{2}$$

where $\tau^{(\alpha)}$ is Schmidt stress with current stress σ; ρ is the density of material after deformation; ρ_0 is the density of material before deformation of 1.78 g/cm^3. According to the abovementioned theory, $\tau^{(\alpha)}$ is equal to the maximum shear component of the Kirchhoff stress which rotates with the lattice, $m^{*(\alpha)}$ is the normal to the slip surface of the slip system in the deformed configuration; $s^{*(\alpha)}$ is the slip direction of the slip system in the deformed configuration. The change of Schmidt stress rate is as follows:

$$\dot{\tau}^{(\alpha)} = m^{*(\alpha)}[\bar{\sigma}^* + \sigma(I{:}D^*) - D^*\sigma + \sigma D^*]s^{*(\alpha)} \tag{3}$$

where $\bar{\sigma}^*$ represents the corotational stress rate on the lattice coordinate axis. The shear strain rate can be achieved through the hardening equation based on the rate-correlated model in this research.

1.2 Rate-correlated hardening of crystalline materials

The rate-correlated plastic limit is rate-independent. According to the Schmidt criterion, the slip rate $\dot{\gamma}^{(\alpha)}$ of α-slip system depends on the corresponding shear stress[22], as follows:

$$\dot{\gamma}^{(\alpha)} = \alpha|\alpha|^{n-1}\dot{\alpha}^{(\alpha)}\left(\frac{\tau^{(\alpha)}}{g^{(\alpha)}}\right) \tag{4}$$

where $\dot{\alpha}^{(\alpha)}$ represents the reference strain rate; $g^{(\alpha)}$ represents the current strength of the slip system; n represents the rate sensitive index. With $n\to\infty$, the strain rate is independent.

The strain hardening can be expressed by Eq.(5), as follows:

$$\dot{g}^{(\alpha)} = \sum\nolimits_{\beta} h_{\alpha\beta}\dot{\gamma}^{(\beta)} \tag{5}$$

where $h_{\alpha\beta}$ is the hardening modulus of slip with α and β slip systems; β represents a different slip system. $h_{\alpha\alpha}$ represents the self-hardening coefficient of α slip system, and $h_{\alpha\beta}$ represents the latent hardening coefficient between α and β slip systems, as follows:

$$h_{\alpha\alpha} = h(\gamma) = h_0\,\mathrm{sech}^2\left|\frac{h_0\gamma}{\tau_s - \tau_0}\right| \tag{6}$$

$$h_{\alpha\beta} = qh(\gamma) \qquad (\alpha \neq \beta) \tag{7}$$

where τ_0 is the critical value of the initial partial shear stress; τ_s is the partial shear stress; h_0 is the hardening coefficient when the material yields; q is a constant; γ is the Taylor cumulative shear strain on all slip systems; $h(\gamma)$ is the intermediate variable. Thus, γ can be expressed by Eq.(8), as follows:

$$\gamma = \sum\nolimits_{\alpha}\int_0^t \left|\dot{\gamma}^{(\alpha)}\right| \mathrm{d}t \tag{8}$$

where t represents the time.

1.3 Expression of volume fraction of twin and grain steering matrix

According to Ref.[27–28], the volume fraction of deformed twin crystal $f_\beta(\tau)$ caused by twinning can be expressed by Eq.(9), as follows:

$$f_\beta(\tau) = \frac{\int_0^\tau \Delta\gamma^\beta(\xi)\mathrm{d}\xi}{\gamma_0} \tag{9}$$

where τ and ξ are time variables; γ_0 is the twin shear strain of AZ31 magnesium alloy[29].

When the cumulative sum of volume fractions of deformed twins in all twin systems $f(\tau)$ is greater than the turning threshold, the twin crystals completely replace the parent grains. The grains are turned along the direction of the largest twin system in the twin crystals, and the turned twin crystal orientation e_{tw} is as follows:

$$e_{tw} = (2n \otimes n - 1)e_{mt} \tag{10}$$

where e_{mt} is the crystal orientation matrix of the untwinned parent grains.

2 Experiment and Simulation

2.1 Experiment

Extruded AZ31 magnesium alloy bar with the diameter of 40 mm was used in this research. The compression specimen of 8 mm×8 mm×12 mm was cut along the radial and axial directions, as shown in Fig. 1. TD, RD, and AD represent the transverse direction, rolling direction, and advanced direction, respectively. The loading direction was along the side with 12 mm in length of each specimen. The compression experiments were conducted on WDW-E100D electronic universal testing machine. The deformation degree was 4% and 8% at room temperature, and the selected strain rate was 10^{-3} s^{-1}. Fig. 2 shows EBSD microstructure of the transverse section (TD-RD). It can be observed that the microstructure is composed of isometric crystals with obviously different sizes. Most grains are distributed at the grain boundaries, indicating that the alloy bar undergoes dynamic recrystallization during the hot extrusion molding process, and the initial grains gradually change to the isoaxial crystals[30].

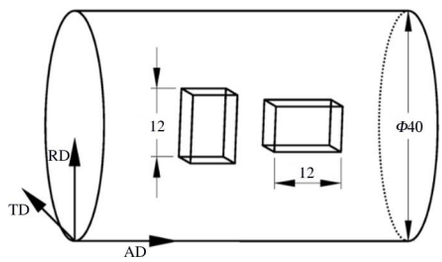

Fig.1 Schematic diagram of compression specimen

In this research, the crystallographic orientation was obtained from EBSD analysis for the rate-correlated crystal plasticity finite element model. Three groups of Euler angles were obtained. According to Eq. (11) [31], the Euler angle is transformed into the cosine form of the crystal coordinate system in the macro-coordinate system. Thus, the texture can be predicted, as follows:

$$g=\begin{bmatrix}\cos\varphi_2 & \sin\varphi_2 & 0\\ -\sin\varphi_2 & \cos\varphi_2 & 0\\ 0 & 0 & 1\end{bmatrix}\begin{bmatrix}1 & 0 & 0\\ 0 & \cos\Phi & \sin\Phi\\ 0 & -\sin\Phi & \cos\Phi\end{bmatrix}\begin{bmatrix}\cos\varphi_1 & \sin\varphi_1 & 0\\ -\sin\varphi_1 & \cos\varphi_1 & 0\\ 0 & 0 & 1\end{bmatrix}=\begin{bmatrix}u & r & h\\ v & s & k\\ w & t & l\end{bmatrix} \tag{11}$$

where φ_1, φ_2, and Φ are the Euler angles; u, r, h, v, s, k, w, t, and l represent the grain orientation.

2.2 Crystal plasticity finite element simulation

Fig. 3 shows the construction process of microstructure model. Because the crystal plasticity constitutive model was established based on rate-correlated mode in this research, the initial microstructure was constructed by the Voronoi method, and the crystallographic orientation was obtained from experiment. The Euler angles of 1500 sets with the same volume fraction were selected, and the Euler spatial segmentation method was used to generate the initial orientation for the model. Then, the X, Y, and Z axes correspond to RD, TD, and AD, respectively. According to the number of grains required for the model and the average grain size measured by the experiment, the crystal plasticity finite element model was established. The model size was 0.4 mm× 0.4 mm×0.6 mm and the model included 1500 units. Each unit represented a grain and different colors reflected different orientations. Therefore, the simulation model was established and the accurate prediction of the deformation texture of the magnesium alloy during compressive process was realized by

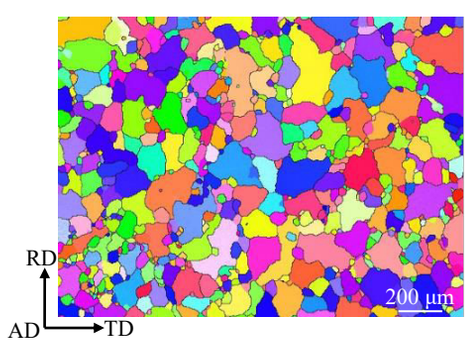

Fig.2 EBSD microstructure of AZ31 magnesium alloy

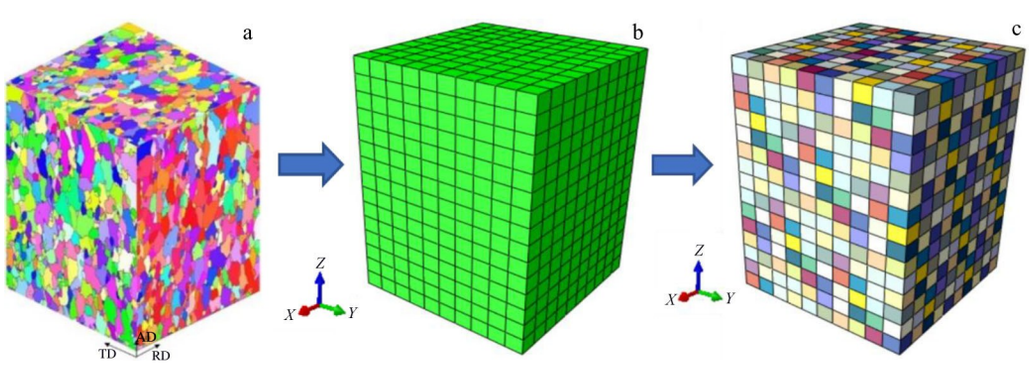

Fig.3 Schematic diagrams of microstructure model construction: (a) 3D EBSD microstructure; (b) 3D finite element model; (c) 3D simulated grain morphology

UMAT in the finite element software.

3 Results and Discussion

Fig. 4 shows the stress distribution nephograms of constitutive models along radial and axial directions during the compressive process. It can be seen that the stress distribution inside and between the grains is uneven: the stress at the grain boundary and inside the grains is increased with increasing the deformation.

Fig. 5 shows the true stress-true strain curves of alloy specimens along the axial and radial directions after different deformation processes. During the compression along *Z*-axis, the stress continues to rise, and the dislocation slip also increases. When the dislocation slip of the initial slip system increases to a certain extent, the radial yield strength and tensile strength are lower than the axial yield strength and tensile strength. The difference in initial texture leads to the obvious anisotropy of compression behavior of AZ31 alloy. Therefore, an appropriate initial texture can greatly improve the forming and service properties of wrought magnesium alloys.

Fig. 6 shows the texture evolution in AZ31 alloy specimen obtained along axial direction during compression process. It can be seen that the simulation results of crystal plasticity finite element model are in good agreement with the experiment results, indicating that the crystal plasticity finite element model can accurately predict the texture evolution process of AZ31 magnesium alloys.

According to Fig. 6, because the initial texture is representative, the simulation results are quite accurate. It is found that a large number of grains along *Z*-axis in the alloy bar are parallel to the axial direction, showing a strong basal texture. When the deformation increases from 0% to 4%, the grains at different positions rotate of a large angle, and the pole density of the {0001} basal texture is dispersed along the positive and negative directions of radial direction. The pole density of the $\{11\bar{2}0\}$ and $\{10\bar{1}0\}$ basal textures changes along the axial direction due to the angular rotation of grains caused by twinning[32]. With increasing the deformation from 4% to 8%, the texture strength of the {0001}, $\{11\bar{2}0\}$, and $\{10\bar{1}0\}$ basal planes is all increased, the pole density does not shift significantly, and the crystals appear in the crystal. The grain tends to be orderly arranged to a certain extent. This is because during the plastic deformation, the slip occurs along the most densely packed plane of atoms, and the crystal rotates together with the slip plane during the slip process, which causes the orientation of grains in the crystal to concentrate along a certain direction, thus forming a texture.

Fig. 7 shows the texture evolutions of {0001}, $\{11\bar{2}0\}$, and $\{10\bar{1}0\}$ basal planes in AZ31 alloy specimen obtained along radial direction during compression process. The {0001} base surface rotates perpendicular to the radial direction. With increasing the deformation, the base surface rotates around the stress direction, the base surface of most grains perpendicular to the compression direction remains, and the polar density of the $\{11\bar{2}0\}$ and $\{10\bar{1}0\}$ base textures is continuously offset in the axial direction[33].

Fig. 8 shows the volume fractions of activated twin crystals

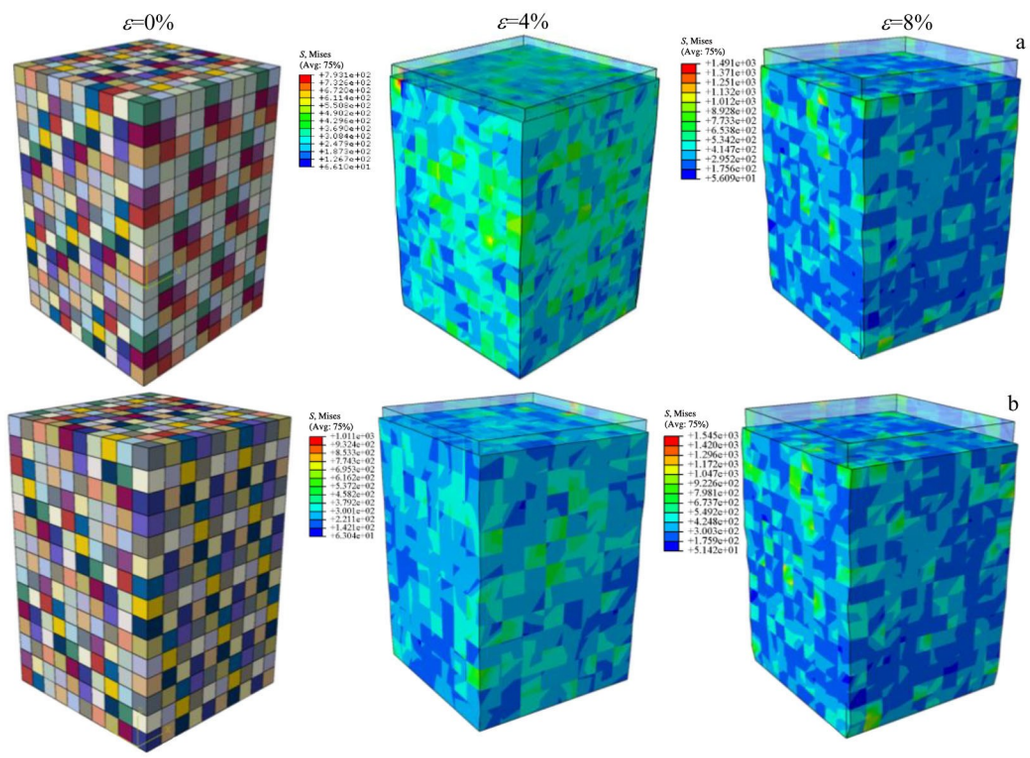

Fig.4 Cloud maps of stress distributions of constitutive models along radial direction (a) and axial direction (b) during compressive process

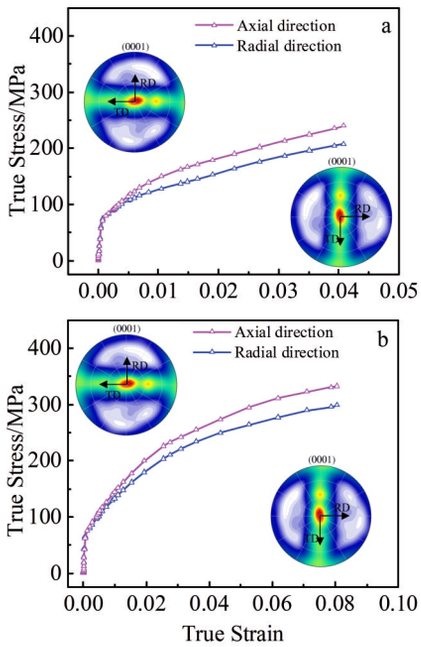

Fig.5 True stress-true strain curves of AZ31 magnesium alloys during compressive deformation of 4% (a) and 8% (b)

in AZ31 magnesium alloys. The twins continuously form inside the grains during compression along the *Z*-axis. With increasing the deformation, the volume fractions of twin crystals is increased, and the grain orientation is changed by the twinning, which is harmful to slip or twinning. The crystallographic orientation becomes favorable, which stimulates the further slip and promotes the continuous plastic deformation.

Fig. 9 shows the volume fraction curves of twin crystals. When the deformation is 4%, the volume fraction of activated twin crystal along axial direction is about 5%, and that along the radial direction is about 40%. When the deformation is 8%, the volume fraction of activated twin crystal along axial direction is 10%, and that along the radial direction is about 70%, suggesting that the volume fraction of twin crystal along radial direction is significantly higher than that along the axial direction. In addition, the higher the volume fraction of radial activated twin crystals, the lower the volume fraction of axial activated twin crystals. During the axial plastic deformation, due to the grain orientation and great change in magnesium alloy, a small number of twin crystals nucleate inside the grains. During the radial plastic deformation, the twin behavior conforms to the Schmidt factor law: the grains with large Schmidt factor preferentially nucleate, and the larger the number of nuclei, the higher the volume fraction of twin grains. Besides, the points of obvious twin crystal appearance in the simulation coincide with those of stress mutation. When the volume fraction of twin crystals reaches about 0.02, the stress changes abruptly. The stress growth rate is reduced sharply with increasing the strain. At this time, the crystal orientation changes, which further stimulates the slip and promotes the continuous plastic deformation. This result reflects the influence of the coupling effect of slip and twinning mechanisms on the mechanical properties of alloys.

Fig. 10 shows the grain boundary distributions of AZ31 magnesium alloys obtained along axial direction and radial direction after compressive deformation of 8%. The grain boundary of misorientation angle of 86°±5° is defined as the stretched twin grain boundary, as indicated by red lines in Fig. 10. It can be seen that the axial tensile twin crystals are significantly less than the radial ones, and the simulated volume fraction of activated twin crystals is consistent with the experiment result, which further verifies the accuracy of simulation model. It is also found that the ratio of the small angle grain boundaries of the radial specimen is significantly reduced, which is attributed to the higher volume fraction of the tensile twin crystals, indicating that the main deformation

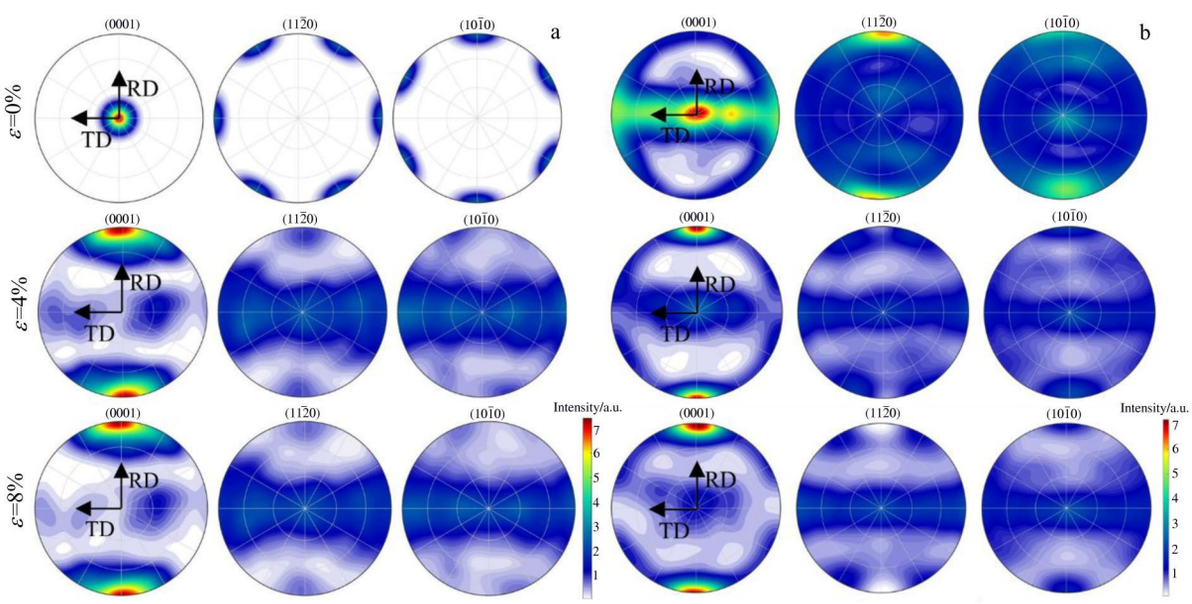

Fig.6 Simulated (a) and experimental (b) texture evolution of AZ31 magnesium alloys obtained along axial direction

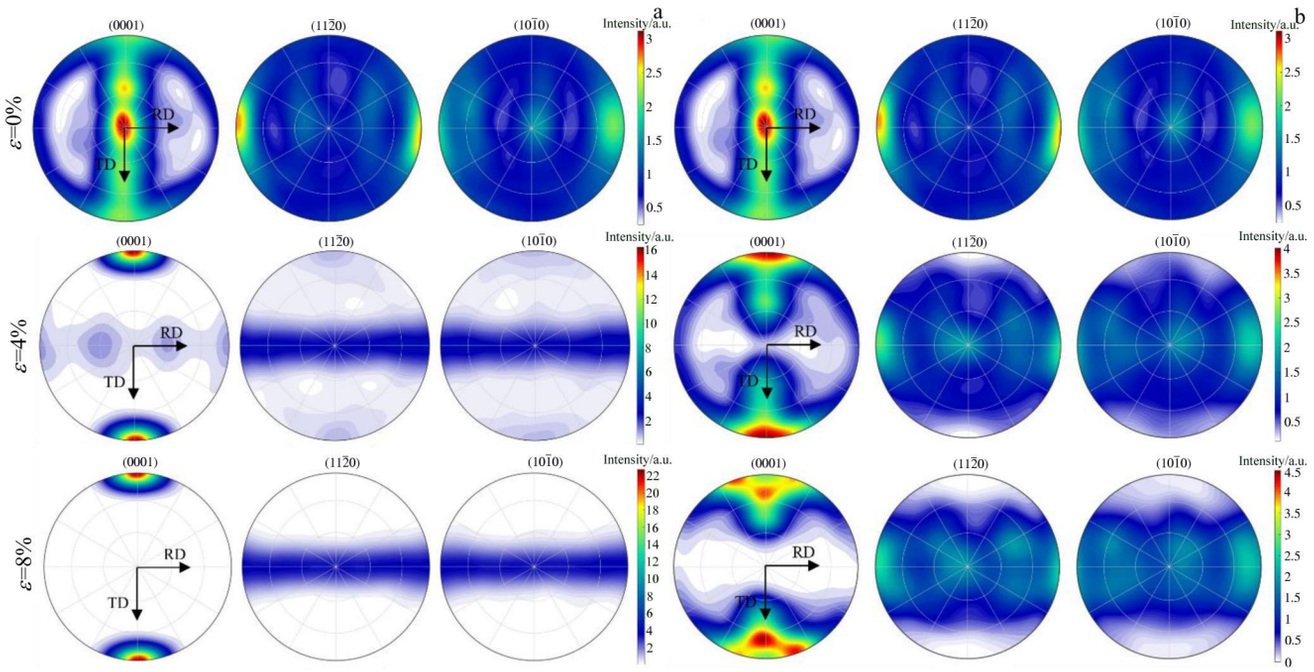

Fig.7 Simulated (a) and experimental (b) texture evolution of AZ31 magnesium alloys obtained along radial direction

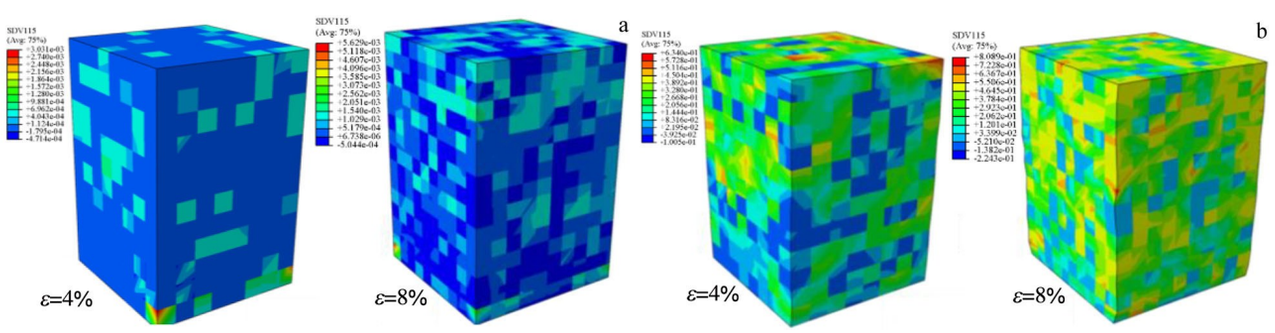

Fig.8 Volume fractions of activated twin crystals in AZ31 magnesium alloys obtained along axial direction (a) and radial direction (b) after compression

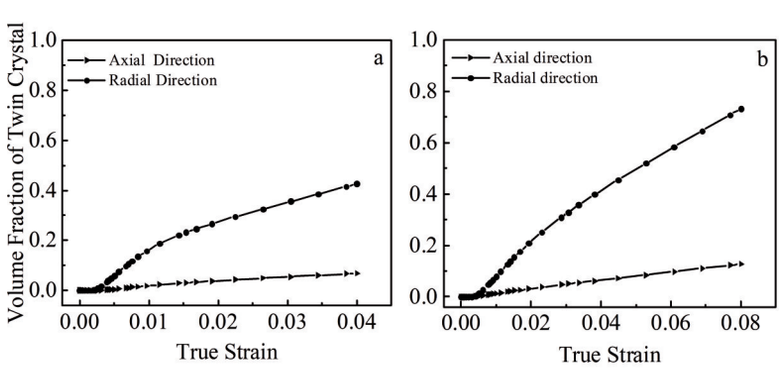

Fig.9 Volume fraction curves of activated twin crystals of AZ31 magnesium alloys obtained along axial direction (a) and radial direction (b) after compression

mechanism in the later deformation stage is tensile twinning rather than slip. This is because the slip can produce a large number of small angle grain boundaries. Thus, the reduced small angle grain boundaries cannot be caused by the slip.

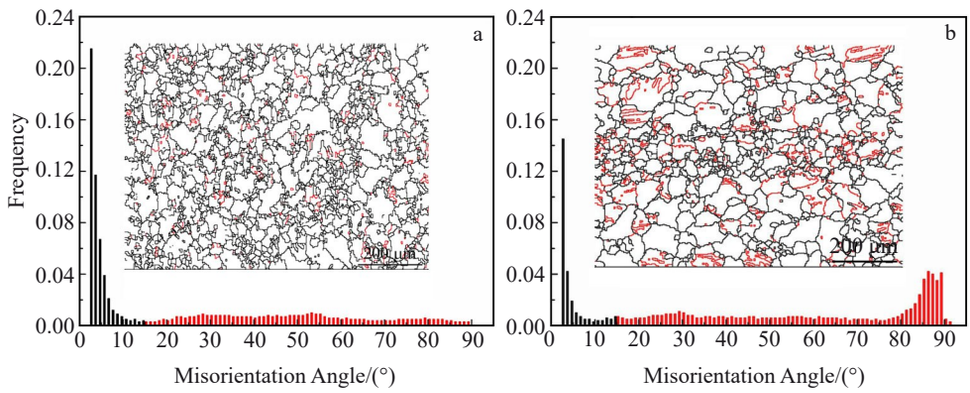

Fig.10 Grain boundary distributions of AZ31 magnesium alloys obtained along axial direction (a) and radial direction (b) after compressive deformation of 8%

4 Conclusions

1) Based on the rate-correlated crystal plasticity theory, a magnesium alloy model with different textures is constructed, including the slip and twinning mechanisms, and the volume fraction of twin crystals is introduced.

2) The plastic behavior of crystals largely depends on the initial texture of alloys. The difference in initial textures leads to the anisotropy of compressive plastic deformation behavior. The radial compressive yield strength and tensile strength are low, and the axial compressive yield strength and tensile strength are high.

3) During the compressive plastic deformation process, with increasing the deformation, the volume fraction of activated twin crystals is increased. The higher the volume fraction of radial activated twin crystals, the lower the volume fraction of axial activated twin crystals.

4) The points of obvious twin crystal appearance in the simulation coincide with those of stress mutation. When the volume fraction of twin fraction reaches about 0.02, the stress changes abruptly. The stress growth rate is reduced sharply with increasing the strain. At this time, the crystal orientation changes, which reflects the influence of the coupling effect of slip and twinning mechanisms on the mechanical properties of alloys.

References

1 Li Yuyu, Yang Bowen, Han Tingzhuang *et al*. *Materials Science and Engineering A*[J], 2022, 845: 143 234

2 Trang T T T, Zhang J H, Kim J H *et al*. *Nature Communications* [J], 2018, 9(1): 2522

3 Hu Hongjun. *Rare Metal Materials and Engineering*[J], 2021, 50(2): 416

4 Xue Chun, Chu Zhibing, Su Hui *et al*. *Rare Metal Materials and Engineering*[J], 2020, 49(12): 4041

5 Liu Shuaishuai, Liu Han, Chen Xiang *et al*. *Journal of Materials Science and Technology*[J], 2022, 113: 271

6 Chu Zhibing, Su Hui, Li Wei *et al*. *Rare Metal Materials and Engineering*[J], 2020, 49(9): 3265

7 Huang Xinde, Xin Yunchang, Cao Yu *et al*. *Journal of Materials Science and Technology*[J], 2022, 109: 30

8 Su Hui, Chu Zhibing, Xue Chun *et al*. *Materials Research Express*[J], 2020, 7(8): 86 503

9 Xiong Hanqing, Wu Yiping, Jia Yuzhen *et al*. *Rare Metal Materials and Engineering*[J], 2020, 49(2): 429

10 Hou Dewen, Zhu Yuzhi, Wen Haiming *et al*. *Materials Science and Engineering A*[J], 2021, 823: 141 748

11 Taylor G I, Elam C F. *Proceedings of the Royal Society of London*[J], 1923, 102(719): 643

12 Asaro R J, Rice J R. *Journal of the Mechanics and Physics of Solids*[J], 1977, 25(5): 309

13 Asaro R J. *Journal of Applied Mechanics*[J], 1983, 50(4): 921

14 Peirce D, Asaro R J, Needleman A. *Acta Metallurgica*[J], 1982, 30(6): 1087

15 Hill R, Rice J R. *Journal of the Mechanics and Physics of Solids* [J], 1972, 20(6): 401

16 Mareau C, Daymond M R. *Acta Materialia*[J], 2010, 58(9): 3313

17 Weber G G, Lush A, Zavaliangos A *et al*. *International Journal of Plasticity*[J], 1990, 6(6): 701

18 Nielsen K L Niordson C F. *Journal of the Mechanics and Physics of Solids*[J], 2014, 63: 113

19 Li Heng, Zhang Zhao, Yang Heng *et al*. *Forging Technology*[J], 2021, 46(4): 11 (in Chinese)

20 Shi Dongfeng, Liu Tianmo, Wang Tianyu *et al*. *Journal of Alloys and Compounds*[J], 2017, 690: 699

21 Wang M, Xu X Y, Wang H Y *et al*. *Acta Materialia*[J], 2020, 201: 102

22 Lan Y T, Zhong X C, Quan G F *et al*. *Transactions of Nonferrous Metals Society of China*[J], 2015, 25(1): 249

23 Su Hui, Chu Zhibing, Xue Chun *et al*. *Rare Metal Materials and Engineering*[J], 2021, 50(10): 3446

24 Ganapathysubramanian S, Zabaras N. *Computer Methods in Applied Mechanics and Engineering*[J], 2004, 193(45–47): 5017

25 Ganapathysubramanian S, Zabaras N. *International Journal of Plasticity*[J], 2005, 21(1): 119

26 Wang Wenbiao. *Research on the Mechanism of Microstructure and Texture Evolution of Polycrystalline Copper During Cold Rolling*[D]. Chongqing: Chongqing University of Technology, 2019 (in Chinese)

27 Rice J R. *Journal of the Mechanics and Physics of Solids*[J], 1971, 19(6): 433

28 Sun Chaoyang, Guo Xiangru, Huang Jie *et al*. *Acta Metallurgica Sinica*[J], 2015, 51(3): 357 (in Chinese)

29 Chino Y, Kimura K, Hakamada M *et al*. *Materials Science and Engineering A*[J], 2008, 485(1–2): 311

30 Song Guangsheng, Zhang Jianqiang, Zhang Shihong. *Rare Metal Materials and Engineering*[J], 2020, 49(1): 288 (in Chinese)

31 Xia Q X, Yuan S, Xiao G F *et al*. *Materials Today Communications*[J], 2021, 27: 102 469

32 Song Guangsheng, Zhang Jianqiang, Niu Jiawei *et al*. *Rare Metal Materials and Engineering*[J], 2019, 48(11): 3563 (in Chinese)

33 Wang Zhongtang, Yan Cao, Song Guangsheng *et al*. *Rare Metal Materials and Engineering*[J], 2012, 41(2): 221 (in Chinese)

初始织构对AZ31镁合金孪生和织构演化的影响

杨博文，马川川，薛　春，拓雷锋，桂海莲，楚志兵

(太原科技大学 材料科学与工程学院，山西 太原 030024)

摘　要：为研究AZ31镁合金变形孪晶和塑性各向异性，基于率相关晶体塑性本构理论，采用有限元方法建立了具有不同初始织构的镁合金模型（包含滑移和孪生变形机制），并引入孪晶体积分数，研究其压缩过程中织构演变、孪生和力学性能之间的关系。结果表明：晶体的塑性行为在很大程度上取决于初始织构，初始织构的差异导致了压缩行为的明显各向异性，轴向屈服强度和抗拉伸强度高，径向屈服强度和抗拉伸强度低。压缩塑性变形过程中随着变形量的增加，激活孪晶体积分数增高，且径向压缩激活孪晶体积分数越高，轴向压缩激活孪晶体积分数越低。模拟中出现明显孪晶的点与应力突变的点相吻合，当孪晶体积分数达到一定值时，应力发生突变，此时晶体取向发生显著变化，新的滑移系启动，反映了滑移和孪晶机制耦合对AZ31镁合金力学性能的影响。

关键词：AZ31镁合金；晶体塑性有限元；初始织构；孪晶；力学性能

作者简介：杨博文，男，1996年生，硕士，太原科技大学材料科学与工程学院，山西 太原 030024，E-mail：885609031@qq.com